Environ. Sci. Technol. **2001**, *35,* 4834−4848

A 3D Eulerian Source-Oriented Model for an Externally Mixed Aerosol

MICHAEL J. KLEEMAN*,† AND GLEN R. CASS‡,#

Department of Civil and Environmental Engineering, University of California, Davis, California 95616, and School of Earth and Atmospheric Sciences, Georgia Institute of Technology, Atlanta, Georgia 30332

A 3D Eulerian source-oriented model for an externally mixed aerosol is developed and then used to compute the contribution that different emission sources make to regional fine particle concentrations in the South Coast Air Basin surrounding Los Angeles, CA, on September 25, 1996. The model simultaneously tracks fine particle concentrations (PM2.5), inhalable particle concentrations (PM10), ozone, and other gaseous pollutant concentrations yielding a tool that can be used to study the control of all of the regulated contaminants in the atmosphere within a single unified framework. Model predictions identify geographical areas that are influenced by PM2.5 associated with crustal material other than paved road dust, paved road dust, diesel engines, food cooking, noncatalyst equipped gasoline engines, catalyst-equipped gasoline engines, combustion of high sulfur-content fuel, other primary particle sources, sea salt, and marine background sulfate particles. The contribution that each of these source types makes to regional fine particle concentrations is distinct, reflecting the unique chemical composition, spatial distribution, and diurnal trends of primary emissions. The single largest contribution to regional PM2.5 in the South Coast Air Basin surrounding Los Angeles is associated with the accumulation of secondary ammonium nitrate on background marine sulfate particles. This pattern indicates that control of PM2.5 concentrations in Los Angeles must be accomplished through a program that includes both reductions in the emissions of gaseous precursors of secondary PM2.5 as well as control of primary particle emissions.

1. Introduction

Atmospheric particles with aerodynamic diameter less than 2.5 μm (PM2.5) have been implicated in adverse health effects (*1*, *2*), visibility reduction (see for example refs *3* and *4*), and global climate change (*5*). The United States Environmental Protection Agency (US EPA) has recently adopted a National Ambient Air Quality Standard (NAAQS) that limits the atmospheric concentrations of PM2.5, but the most efficient approach to reducing PM2.5 concentrations is not obvious. A variety of sources release fine particles to the atmosphere including automobiles, heavy-duty trucks, wood burning, and food cooking. PM2.5 can also form in the atmosphere through chemical reactions that convert gaseous pollutants to semivolatile products that can partition into the particle phase. Emissions controls applied to any of these potential PM2.5 source categories could involve large economic and social consequences. At the same time, requirements exist for emissions control programs that will reduce particle concentrations in sizes less than 10 μm particle diameter (PM10), while further control of ozone concentrations is required in many metropolitan and some rural areas. The ozone and particle control problems are intimately linked to each other because the oxides of nitrogen and organic vapors that lead to ozone formation also can lead to secondary aerosol nitrate and secondary organic aerosol production as well. Faced with this complexity, decision makers need new tools that clearly show the relationship between emissions sources and airborne pollutant concentrations in both the gas and particle phases.

Recently, a mechanistic air quality model has been developed that can directly show how particles emitted from hundreds of different sources influence the particle size distribution and chemical composition seen at receptor air monitoring sites. This model uses a fundamental mathematical representation of emissions, atmospheric turbulence, dry deposition, gas-phase chemical reaction, aqueous-phase chemical reaction, and gas-to-particle conversion (*6*) to understand how different sources contribute to the size and composition distribution of atmospheric particles (*7*, *8*) and to predict how different emissions control strategies will affect the properties of the airborne particles (*9*). Because the gas-phase chemical reactions in the atmosphere surrounding the particles are represented explicitly, the model can be used to study ozone formation and control as well. Since the particle size distribution is represented explicitly up to particle sizes of 10 μm particle diameter, the model can track source contributions to PM10 concentrations. The air quality calculations conducted to date using this model have been based in a Lagrangian framework in which the atmospheric processes within individual air parcels were followed in a coordinate system that moved with the average fluid velocity. The Lagrangian framework has proven to be extremely useful because it provides a basis for confirming the scientific merit of the model within a format that runs very quickly on the computer and thus that can be tested extensively and rapidly. But use of the Lagrangian framework limits pollutant concentration predictions to a single location at any given time. Many thousands of air parcels would need to be followed to characterize the spatial distribution of pollutants within a large airshed. Also, the Lagrangian framework does not capture the effects of vertical wind shear and turbulent diffusion in the horizontal plane (*10*). Although these processes are often minor, they may influence pollutant concentrations during certain atmospheric conditions.

The focus of the current study is to place the source-oriented model for an externally mixed aerosol within a 3D Eulerian framework so that the spatial distribution of the source contributions to regional PM2.5 concentrations can be evaluated. Virtually all other 3D Eulerian air quality models that have been demonstrated to date approximate airborne particulate matter as an internal mixture using either a sectional representation (*11*−*18*) or using log-normal modes (*19*, *20*). One Eulerian air quality model (*21*) used an approach similar to that demonstrated previously in the Lagrangian formulation of the source-oriented external mixture air quality model (*6*−*9*), but only three simplified source categories were tracked through the modeling framework,

* Corresponding author phone: (530)752-8386; fax: (530)752-7872; e-mail: mjkleeman@ucdavis.edu.
† University of California.
‡ Georgia Institute of Technology.
# Deceased.

10.1021/es010886m CCC: $20.00
Published on Web 11/06/2001

and no attempt was made to evaluate model results against aerosol measurements. The model described in the current paper therefore represents the most detailed calculation to date of the evolution of airborne particulate matter in an urban region.

As a source apportionment tool, the 3D Eulerian source-oriented external mixture air quality model can determine source contributions to size distribution of airborne particulate matter on a regional scale. The new model can differentiate between particles released from different sources at different locations/times, and it can accurately determine the amount of secondary particulate matter that has built up on those particles. Theoretically, the model can be used to differentiate between source contributions from many thousands of different sources, greatly exceeding the resolution of traditional statistical source apportionment techniques.

In the sections below, the formulation of the 3D model is described, and the results of model predictions of ozone and fine particle concentrations in Southern California are presented.

2. Background

The air quality model developed in the current study is based on the California Institute of Technology (CIT) family of 3D Eulerian and Lagrangian atmospheric chemistry models. There are now many official (and unofficial) versions of this model in existence; to set the stage for the current study, the evolution of the CIT airshed model that forms the framework for the current work is briefly described.

One of the first atmospheric chemistry models was developed in the early 1970s at Caltech and at Systems Applications Incorporated. Referred to as the Urban Airshed Model (UAM (*22*−*24*)) it was used to examine the effect of the 1977 EPA ozone control plan for the Los Angeles Basin based on the meteorological conditions of September 29, 1969 (*25*). By the early 1980s a new comprehensive modeling system, the CIT model (*26*, *27*), was developed with an updated chemical mechanism (*28*, *29*) and improved input data generation (*30*, *31*) and was used to model air quality over the period June 26−28, 1974.

The chemistry of nitrogen-containing air pollutants within the CIT family of air quality models was expanded to include more gaseous species, additional nighttime reactions, and a thermodynamic equilibrium treatment of ammonium nitrate aerosol production (*32*). This version of the CIT airshed model and its associated August 30, 1982−September 1, 1982 model performance evaluation data set were used to study the control of nitrogen-containing pollutants (*33*), the spatial patterns in pollutant responses to emission reductions (*34*), the effect of alternate fuel use in motor vehicles (*35*, *36*), and modeling and control of the deposition of nitrogen-containing air pollutants (*37*). The CIT airshed model was further updated to study the detailed chemistry of speciated organic gas-phase pollutants (*38*, *39*) during the Southern California Air Quality Study (SCAQS) episode of August 26−28, 1987.

Detailed thermodynamic calculations describing the kinetics of the formation of inorganic aerosol species in the atmosphere were added to the CIT family of air quality models by Wexler and Seinfeld (*40*), and the first prediction of secondary organic aerosol formation was incorporated into the CIT family of air quality models by Pandis et al. (*41*). An externally mixed aerosol representation in which particles of the same size having different chemical compositions are tracked separately was incorporated into the CIT Lagrangian air quality model by Kleeman et al. (*6*). The externally mixed version of the CIT Lagrangian model was used to determine how different sources contribute to the size and composition distribution of airborne particles at target receptor sites in the South Coast Air Basin of Los Angeles on August 28, 1987 (*6*, *7*) and September 23−25, 1996 (*8*).

3. Model Formulation

The air quality model developed in the present study represents atmospheric processes at their fundamental level so that the effects of changing meteorological conditions and emissions on the concentration of airborne pollutants can be predicted. The first-order processes that dominate air quality at the urban and regional scale are emissions, advection, diffusion, and deposition of airborne pollutants. The concentrations of secondary pollutants such as ozone and secondary particulate matter also are influenced by higher order atmospheric processes including gas-phase chemical reactions, particle-phase chemical reactions, and phase-transfer processes (gas to particle partitioning). Equation 1 describes the overall mathematical representation of these atmospheric processes in a highly simplified form

$$\frac{\partial C_i}{\partial t} + \nabla \cdot u C_i = \nabla K \nabla C_i + E_i - S_i + R_i^{gas}(C) + R_i^{part}(C) + R_i^{phase}(C) \quad (1)$$

where C_i is the concentration of gas- or particle-phase species at a particular location as a function of time t, u is the wind vector, K is the turbulent eddy diffusivity tensor (assumed to be diagonal), E_i is the emissions rate, S_i is the loss rate, R_i^{gas} is the change in concentration due to gas-phase reactions, R_i^{part} is the change in concentration due to particle-phase reactions, and R_i^{phase} is the change in concentration due to phase change. Many of the terms shown on the right side of eq 1 are evaluated in separate steps within the air quality model (operator splitting) that require multiple layers of implicit iteration to achieve convergence. The details of the solution methods for each of these numerical procedures have been provided elsewhere (see references in section 2), and so only those portions of the model that have been updated in the current work are described here.

3.1. Advection and Turbulent Mixing. For use in the present work, the advection operator used in the base CIT airshed model was updated from the Finite Element Method (FEM) described by McRae et al. (*26*) to the more exact Accurate Space Derivative Method (ASD) (*42*) coupled with a Forester Filter (*43*) to reduce numerical noise. While the ASD method is more numerically intensive than the FEM approach, the overall computational burden is still minor relative to that imposed by the particle chemistry segments of the model.

The representation of vertical turbulent mixing in the original version of the CIT airshed model was based on a first-order turbulent closure scheme of the form

$$<u'_z c'> = -K_{zz}\frac{\partial c}{\partial z} \quad (2)$$

where u_z' is the turbulent component of velocity in the vertical direction z, c' is the turbulent component of concentration c, the angle brackets are the ensemble-averaging operator, and K_{zz} is a turbulent eddy diffusivity in the vertical direction that changes in response to different atmospheric stability conditions. The empirically derived equations originally used in the CIT model to describe the behavior of K_{zz} were parameterized largely based on experiments conducted in remote locations that were not influenced by urban heat island effects and mechanical mixing caused by on-road vehicles. The use of this representation results in an under prediction of atmospheric mixing during the evening hours in urban locations as described by Harley et al. (*39*) and Kleeman et al. (*8*). In the current study, a minimum value

of K_{zz} is specified that promotes atmospheric mixing up to the base of the temperature inversion during the evening hours.

3.2. Nitrate Formation at Night. It is generally understood that the primary route for nitrate formation in an urban area during the evening is N_2O_5 hydrolysis. Investigators originally postulated a homogeneous gas-phase route for this reaction, but recent studies have determined that the N_2O_5 hydrolysis reaction occurs heterogeneously between gaseous N_2O_5 and particle-bound water. In the current study, the AIM subroutine used to calculate the condensation/evaporation of semivolatile inorganic components (*6*, *40*) was further modified to describe N_2O_5 hydrolysis on wet airborne particles. The rate-limiting step for this process was assumed to be mass transfer limitations associated with gas-phase diffusion and interfacial transfer.

The equation describing the evolution of gas-phase N_2O_5 concentrations due to reaction at the surface of particles is

$$\frac{1}{N_2O_5}\frac{\partial N_2O_5}{\partial t} = -4\pi D_{N_2O_5}\sum_j \frac{Rp^j N^j}{\beta^j_{N_2O_5}+1} \tag{3}$$

$$\beta^j_{N_2O_5} = \frac{4D_{N_2O_5}}{\alpha_{N_2O_5}\hat{c}Rp^j} \tag{4}$$

$$\hat{c} = \sqrt{\frac{8RT}{\pi Mwt_{N_2O_5}}} \tag{5}$$

where $D_{N_2O_5}$ is the gas-phase diffusion coefficient, Rp^j is the radius of wet particle j, N^j is the number concentration of wet particle j, $\alpha_{N_2O_5}$ is the accommodation coefficient for reaction of N_2O_5 molecules on the wet particle surface, $\hat{c}$ is the molecular speed of the N_2O_5 gas molecules, R is the gas constant, T is the ambient temperature, and $Mwt_{N_2O_5}$ is the molecular weight of N_2O_5. The time-scale for the heterogeneous conversion process may be calculated as

$$\tau_{heterogeneous} = \frac{1}{4\pi D_{N_2O_5}\sum_j \frac{Rp^j N^j}{\beta^j_{N_2O_5}+1}} \tag{6}$$

This can be compared to the time scale inferred from the previously assumed homogeneous conversion reaction

$$\tau_{homogeneous} = \frac{1}{H_2O^* k_{N_2O_5}} \tag{7}$$

where H_2O is the concentration of vapor-phase water and $k_{N_2O_5}$ is the effective homogeneous rate constant. Simulations for Southern California that are summarized in Section 4 of the current study revealed very little difference between the new heterogeneous time scale and the original homogeneous time scale for N_2O_5 hydrolysis.

3.3. Secondary Aerosol Formation. The partitioning of semivolatile organic species into the particle phase is accomplished using the partitioning coefficients measured by Odum et al. (*44*) while considering departures from equilibrium associated with the time required for molecules to diffuse through the gas phase and for molecules to cross the gas-particle phase interface. The net equation describing this process is given by

$$\frac{\partial C^j_{org}}{\partial t} = 4\pi D_{org}\frac{Rp^j N^j}{\beta^j_{org}+1}\left(C^{gas}_{org} - \frac{C^j_{org}}{K_{org}M^j_o}\right) \tag{8}$$

where C^j_{org} is the concentration of the organic species associated with particle j, C^{gas}_{org} is the concentration of the organic species in the gas phase, D_{org} is the gas-phase diffusivity of the organic species, K_{org} is the partitioning coefficient for the organic species, and M^j_o is the total amount of organic matter on particle j that is available for partitioning.

The partitioning of semivolatile inorganic species between the gas and particle phases also is described by an equation analogous to eq 8, but the calculation of vapor pressures above the particle surface is accomplished by considering the thermodynamic equilibrium state of each particle as calculated by a modified form of the Aerosol Inorganic Module (AIM) originally developed by Wexler and Seinfeld (*40*). A description of the modifications made to the original AIM approach is provided by Kleeman et al. (*6*).

3.4. General Aerosol Operators. All of the processes that influence airborne particles on the urban and regional scale are included in new 3D source-oriented external mixture model (emissions, advection, turbulent diffusion, dry deposition, gas-phase chemistry, aqueous-phase chemistry, and gas-to-particle conversion). Aerosol processes in the new air quality model are represented using the aerosol operators developed for the Lagrangian version of the model (*6*, *8*). Particles from individual emissions sources are grouped into 10 selected classes: paved road dust, crustal material other than paved road dust, diesel engine exhaust, noncatalyst-equipped gasoline engine exhaust, catalyst-equipped gasoline engine exhaust, food cooking, high sulfur-content fuel combustion, wave-generated sea salt aerosol, background sulfate aerosol, and other particle sources. Particles within each source class are separately tracked through a mathematical simulation of atmospheric advection, diffusion, deposition, and chemical reaction. Particles are not artificially mixed into a single atmospheric particle size and composition distribution (internal mixture), but rather they exist separately from one another and interact only through exposure to the same gas-phase atmosphere. Since the source origin of each airborne primary particle is know, it is possible to examine how particles emitted from different sources are modified in the atmosphere and contribute to the size and composition of particulate matter found at downwind receptor sites.

The current application of the source-oriented model for an externally mixed aerosol does not include nucleation processes since they are usually negligible contributors to fine particle mass in urban areas where large amounts of preexisting particulate matter provide sufficient area for condensation of semivolatile gas-phase species (*11*). Coagulation processes also are not considered in the current implementation because they do not play an important role in shaping the particle mass distribution over a time scale of only a few days (*6*, *11*). A further discussion of the effects of neglecting nucleation and coagulation for the model episode considered in the present analysis may be found in Section 5.2.

3.5. Parallel Implementation. The majority of the computational burden in all mechanistic air quality models that include a description of aerosol processes is associated with aerosol thermodynamic calculations. Because the high-resolution air quality model developed in the current study tracks approximately 19 times more particle-phase information than other aerosol processes air quality models (10 particle classes and 15 particle sizes vs typically one particle class and 8 particle sizes) the computational overhead is proportionally larger. To perform air quality simulations in a practical amount of time the new air quality model is implemented on a parallel computing platform. Separate processors on a host parallel computer solve independent advection and particle-phase operations within each model time step. The simulation described in the following sections

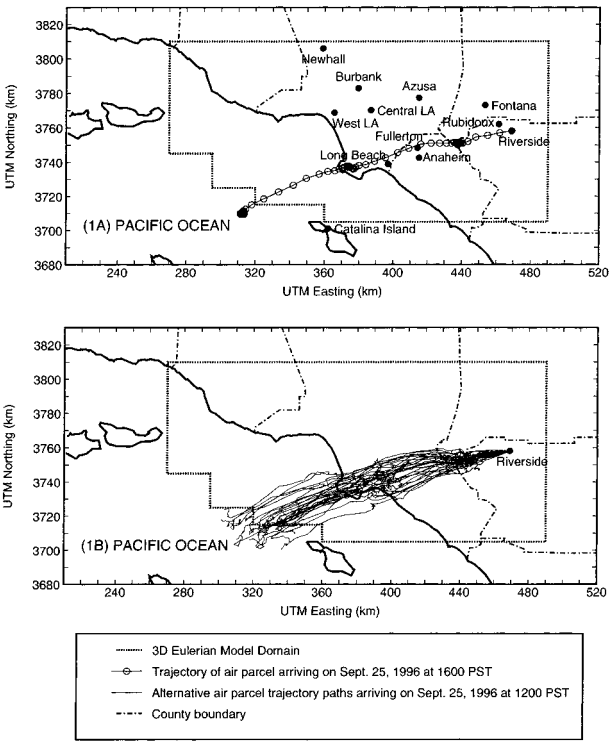

FIGURE 1. Map of the South Coast Air Basin surrounding Los Angeles, CA. The dashed line encloses the computational region for model calculations. The trajectory of the air parcel arriving at Riverside, CA, at 16:00 PST on September 25, 1996 illustrates the general wind pattern during the 3-day study period.

was performed on an 80 node parallel machine where each node consisted of a 466 MHz Intel Celeron processor equipped with 32MB of RAM. Each day of simulation required approximately 2 days of CPU time for the current study.

4. Model Application

3D Eulerian air quality model calculations were performed for September 23−25, 1996 within the region surrounding Los Angeles, CA. The September 23−25, 1996 time period was chosen for model evaluation in the current study because it represents the most recent episode for which the large amount of data (emissions, meteorology, initial conditions, boundary conditions, receptor site concentrations) needed for air quality model evaluation are available. Current model evaluation data sets are required for the development of appropriate emissions control strategies.

Figure 1a shows portions of Ventura County, Los Angeles County, Orange County, San Diego County, Riverside County, and San Bernardino County. The rectangular dashed line in Figure 1a shows the boundary of the computational region used by the model, which corresponds closely to the heavily populated South Coast Air Basin plus a portion of Ventura County. The modeling domain within this region is subdivided into 5 km × 5 km square grid cells in the horizontal direction, with seven levels in the vertical direction. The spacing of the vertical layers is logarithmic with cell depths of 35, 65, 100 m and four additional cells with depth 200 m resulting in a total column depth of 1000 m. The total modeling domain includes 5936 separate computational cells.

4.1. Meteorological Conditions. Surface meteorological conditions within the study domain were measured by a network of routine monitoring stations operated by the South Coast Air Quality Management District, the National Climatic Data Center, and the California Irrigation Management System. Measured values of wind speed (29 sites), wind direction (29 sites), temperature (10 sites), relative humidity (10 sites), total solar radiation (4 sites), and ultraviolet solar radiation (1 site) were used to specify values for these parameters throughout the study region using the interpolation procedure of Goodin et al. (*19*). Wind speed and wind direction above the earth's surface were interpolated based on measurements made using a lower atmospheric radar profiler located at Los Angeles International airport (LAX), and rawinsonde information collected at Edwards Air Force Base, Vandenberg Air Force Base, and San Nicolas Island.

The 3-day air parcel trajectory shown in Figure 1a is provided to illustrate the general airflow pattern during the study period. The air parcel that arrives at Riverside, CA, at 16:00 PST on September 25, 1996 was located over the Pacific Ocean on September 23, 1996. The air parcel then was advected inland where it stagnated just west of Long Beach, CA, on the night of September 23, and between Riverside, CA, and Fullerton, CA, on the night of September 24. The eastward flow pattern illustrated by this trajectory path is typical of the flow pattern found throughout the modeling region during the current study.

Atmospheric mixing depths during the study period were constructed using Holtzworth's method (*45*) based on measured surface temperatures throughout the modeling domain combined with the vertical temperature structure observed by the lower atmospheric radar profiler located at Los Angeles International Airport (LAX). As noted previously (*8*), mixing depths during the study period were large, ranging between 100 m at night to more than 1000 m during the day. The lack of a very low-level atmospheric temperature inversion that traps pollutants close to the earth's surface prevented the development of a region-wide peak pollution event such as those previously studied in the Los Angeles area (*39*). The 3-day episode considered in this study is typical of an "average" air quality event in the South Coast Air Basin during the fall months. As such, it represents the level of air pollution that the approximately 15 million people in that air basin are exposed to on a routine basis.

4.2. Initial and Boundary Conditions. Initial conditions for the model calculations were interpolated based on observed pollutant concentrations within the South Coast Air Basin. Concentrations of routinely monitored gas-phase pollutants (O3, NOx, SOx, CO, CO2, RHC) were interpolated based on measurements made at 28 monitoring sites operated by the South Coast Air Quality Management District (SCAQMD). Initial concentrations of gas-phase nitric acid, gas-phase ammonia, and particle size and composition were specified based on measurements made at Long Beach between 6:00−10:00PST, Fullerton between 10:00−14:00PST, and Riverside between 14:00−18:00PST on September 23, 1996 (*46*). The initial concentrations of nitric acid, ammonia, and initial particle size and composition were back-extrapolated to 0:00PST on September 23, 1996 based on the 4-h measurements described above scaled according to the diurnal profile for these pollutants measured in the South Coast Air Basin between September 8−9, 1993 (*47*).

Boundary conditions on the western edge of the study domain were measured with impactor and filter-based samplers at Santa Catalina Island on September 23, 1996 as described by Hughes et al. (*46*) and Kleeman et al. (*8*). Information on the coarse airborne particles was inferred from the difference between TSP (∼PM30) and PM1.8 measurements. Sodium chloride measurements at Santa Catalina Island were used to describe the size and composition distribution of sea salt particles produced through the action of breaking waves over the open ocean. Sea salt emissions also were specified along the surf-zone within the modeling region based on a detailed sea spray emissions model (*48*).

The concentration and speciation of gas-phase aldehydes on the Western edge of the modeling domain was based on measurements taken at San Nicolas Island in September 1993 (*49*).

4.3. Emissions. Anthropogenic emissions of gas- and particle-phase pollutants were specified using an emissions modeling system described previously (*8*, *50*). In this system, the standard emissions inventories provided by the South Coast Air Quality Management District (SCAQMD) are transformed into detailed emissions inventories for speciated organic gases and particle size/composition.

The three major components of the standard emissions inventory are the mobile source inventory, the point source inventory, and the area source inventory for the study region. The base mobile source emissions inventory provided by the SCAQMD was calculated using the traffic emissions model EMFAC-7G with a day-specific temperature correction for evaporative emissions. The activity data (VMT) and spatial distribution of mobile source emissions was retained, but the actual emissions totals and particle size/composition distributions were recalculated based on mobile source emissions profiles measured during source tests conducted by the Cass research group (*51*−*53*). The mass emissions inventories for area sources and small point sources within the modeling domain were based on the 1995 average-day emissions inventory supplied by the SCAQMD combined with particle size and composition profiles as specified by Kleeman et al. (*8*). The inventory for large point sources used in the current study was based on the 1997 average-day inventory supplied by the SCAQMD again combined with particle size and composition profiles as specified by Kleeman et al. (*8*). The speciation of organic compounds in the emissions processing system is based on the treatment of Harley et al. (*38*, *54*).

Ammonia emissions in the South Coast Air Basin during the study period are based on the 1982 ammonia emissions inventory of Gharib and Cass (*55*) updated to the year 1996 to reflect changes in mobile sources, fertilizer, and livestock emissions (*8*). Biogenic hydrocarbon emissions within the study domain are based on the 1987 SCAQS inventory developed for the late summer of that year. The use of that biogenic emissions inventory during the current study assumes that the distribution and speciation of plants within the study domain have not undergone major changes.

5. Model Results

5.1. Comparison to Measured Data. Figure 2 shows the predicted and observed values of ozone (O3) at Central Los Angeles, Azusa, Fontana, West Los Angeles, Anaheim, Rubidoux, Burbank, and Newhall, CA on September 23−25, 1996. Observed O3 concentrations have an uncertainty of approximately ±15%. O3 concentrations on the western edge of the modeling domain show a less pronounced diurnal variation than O3 concentration profiles at the eastern end of the air basin. Air quality model predictions for peak O3 concentrations match observed values on each day of the simulation and are generally less than 100 ppb. Peak O3 concentrations show good agreement with observations on the third day of the simulation after startup effects have had a chance to dissipate. Nighttime concentrations of O3 are slightly underpredicted at several of the monitoring sites. This condition is caused by fresh emissions of NO into the simulated atmosphere during the evening hours. It is expected that a day-specific emissions inventory with more accurate diurnal variations would correct the ozone under predictions at night.

Model calculations that represent airborne particles using a discrete particle size distribution can be used to predict mass distributions for comparison to filter-based and impactor mass measurements by summing across particle types and/or sizes. Figure 3 shows the predicted concentrations of major components of the airborne particle complex

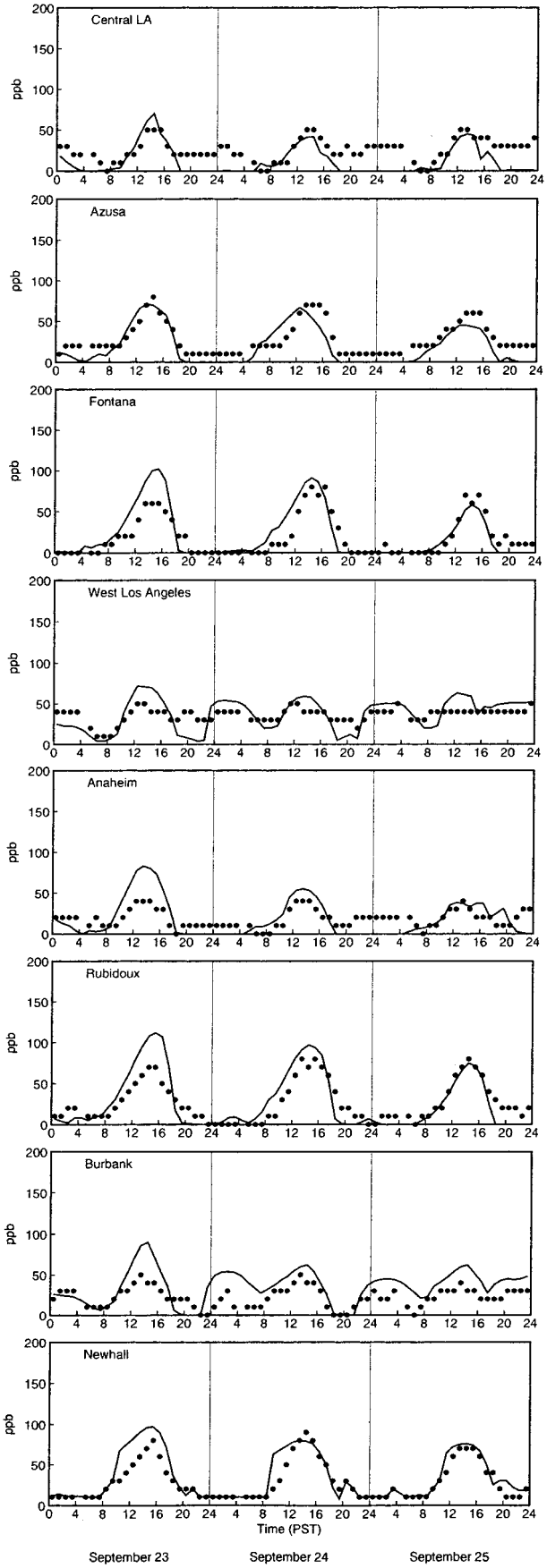

FIGURE 2. Predicted (solid line) and observed (dots) ozone concentrations on September 23−25, 1996.

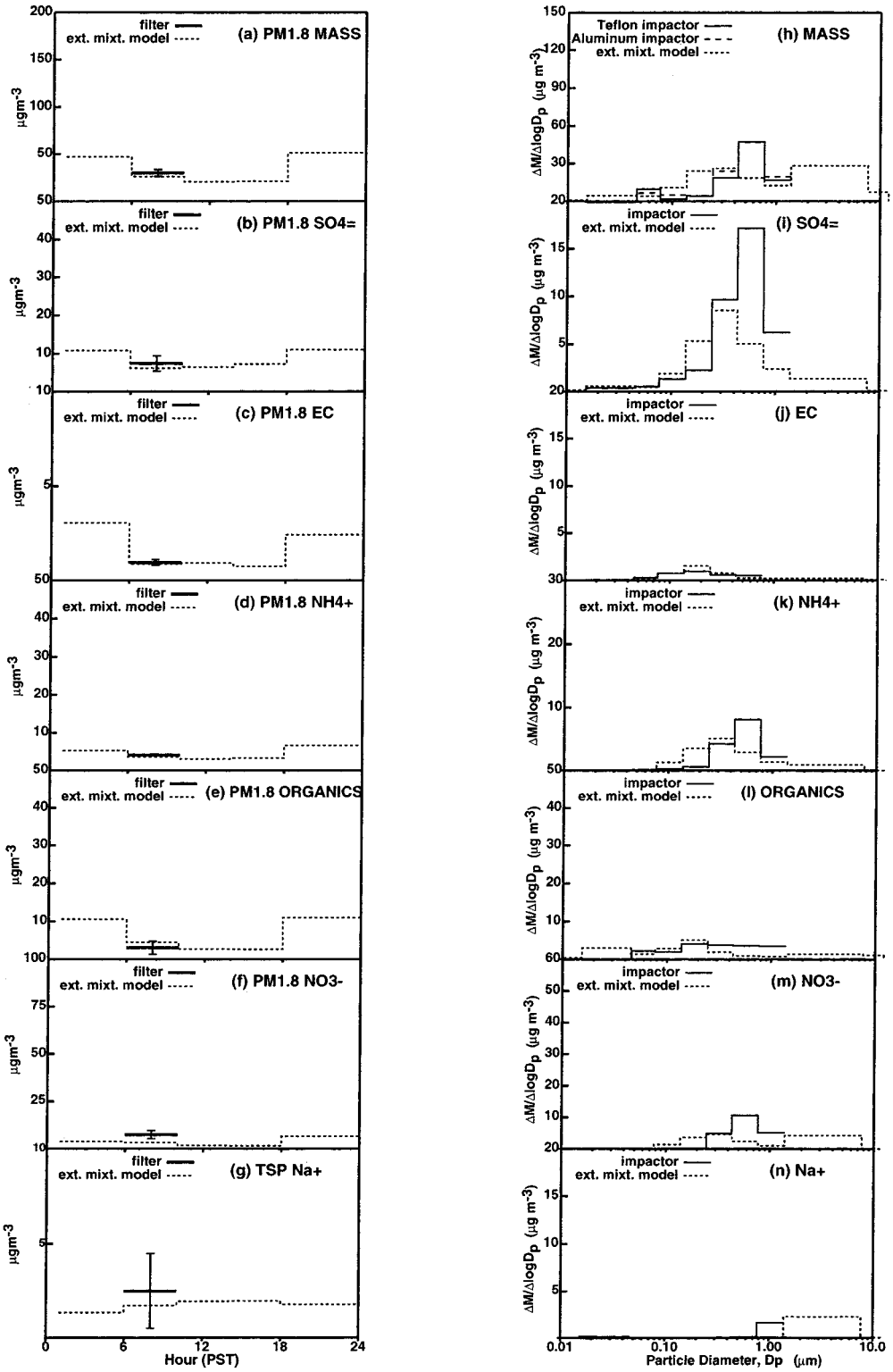

FIGURE 3. Predicted and observed components of airborne particles at Long Beach, CA, on September 24, 1996. Panels a−g illustrate the diurnal profile of PM1.8 particle-phase concentrations, while panels h−n illustrate the size distribution of particle-phase species averaged between 6:00−10:00 h PST. Uncertainty estimates for measured PM1.8 concentrations reflect the difference between collocated filter-based measurements and summed impactor measurements of particle-phase concentrations.

at Long Beach throughout the day on September 24, 1996 along with the measured concentration of particulate matter components collected between 6:00−10:00 PST that day by Hughes et al. (*46*). Model predictions show excellent agreement with filter-based measurements of particulate matter mass in particle sizes smaller than 1.8 μm aerodynamic diameter (PM1.8), sulfate (SO4=), elemental carbon (EC), ammonium ion (NH4+), organics (ORGANICS), and sodium (Na+) (Figures 3a−e,g). Predicted concentrations of PM1.8 nitrate (NO3-) are slightly lower than measured PM1.8 nitrate concentrations. In the present study, particle-phase boundary conditions along the Western edge of the modeling domain are based on a single measurement at Santa Catalina Island collected on September 23, 1996. It is likely that the agreement

between predicted and measured PM1.8 nitrate concentrations at Long Beach could be improved through the use of boundary conditions for airborne particulate matter that had greater time and spatial resolution.

Figures 3h−n show the measured and predicted size distribution of airborne particle components at Long Beach averaged between 6:00−10:00 PST on September 24, 1996. Impactor measurements do not extend above 1.8 μm particle aerodynamic diameter, while model predictions extend up to 10 μm particle diameter. Model calculations predict that the peak in the airborne particle EC and ORGANICS distribution occurs between 0.1 and 0.2 μm matching the observed distribution of carbonaceous aerosol (Figure 3j,l). The predicted peak in the SO4=, NH4+, and NO3- size distribution occurs between 0.25 and 0.45 μm, while the peak in the observed size distribution for these chemical species occurs in the next impactor size bin between 0.45 and 0.9 μm (Figure 3i,k,m). The magnitude of the peak concentration in the predicted SO4= size distribution is lower than the peak concentration in the measured SO4= size distribution, but it should be noted that the predicted amount of sulfate contained in particles with aerodynamic diameter less than 1.8 μm matches the filter-based SO4= measurement (Figure 3b). The amount of Na+ contained in airborne particles with diameter less than 0.9 μm is both predicted and measured to be essentially zero, while the amount of Na+ predicted in particles larger than 1.8 μm matches observed Na+ concentrations in the next size bin down (impactor measurements of Na+ concentrations in particles larger than 1.8 μm are not available).

Figure 4 shows the predicted concentration of the major components of the airborne particle complex at Riverside throughout the day on September 25, 1996. Also shown in Figure 4 is the measured concentration of particulate matter components collected between 14:00−18:00 PST by Hughes et al. (*35*). Model predictions show excellent agreement with filter-based measurements of PM1.8 SO4=, NH4+, NO3-, and Na+ (Figure 4b,d,f,g). PM1.8 EC and ORGANICS concentrations are underpredicted between 14:00−18:00 PST (Figure 4c,e), leading to an under prediction in PM1.8 MASS (Figure 4a). The majority of the particulate EC and ORGANICS in the model calculation are directly emitted from combustion sources, with only minor contributions from secondary formation processes. The underprediction of ORGANICS concentrations at Riverside could be caused by either the underestimation of primary organic carbon particle emissions, the underestimation of secondary organic aerosol formation, or by organic vapor pick-up by the quartz fiber filters used to measure organic aerosol concentrations.

Figures 4h−n show the measured and predicted size distribution of airborne particle components at Riverside averaged between 14:00−18:00 PST on September 25, 1996. Impactor measurements do not extend above 1.8 μm particle aerodynamic diameter, while model predictions extend up to 10 μm particle diameter. The predicted quantities of total fine particulate MASS, SO4=, NH4+, and NO3- are in good agreement with measured values, but the measured particle size distribution is generally shifted to larger particle sizes by one impactor bin (Figures 4h,i,k,m). As was the case for the Long Beach comparison, the amount of Na+ contained in airborne particles with a diameter less than 0.9 μm is both predicted and measured to be essentially zero, while the amount of Na+ predicted in particles larger than 1.8 μm matches observed Na+ concentrations in the next size bin down. The predicted ORGANICS particle size distribution falls below the observed values for the reasons discussed above.

Uncertainty in the measured concentrations shown in Figures 3 and 4 can be calculated directly as the difference between collocated measurements when they are available. In the present study, the impactor results shown in Figures 3 and 4 can be summed across all particle sizes to produce a PM1.8 concentration that was collocated with the filter-based measurement. Comparison of concentrations measured using different collection techniques captures the effect of sampling biases such as loss of volatile species from impactor stages. The difference between the filter-based PM1.8 measurements and impactor PM1.8 measurements for each chemical species is used as an estimate of uncertainty about the PM1.8 filter measurements shown in Figures 3 and 4. Results indicate that model predictions fall within the uncertainty range of all PM1.8 measurements with the exception of an underprediction of nitrate concentrations at Long Beach between 6:00−10:00 PST on September 24, 1996, and an underprediction of elemental/organic carbon concentrations at Riverside between 14:00−18:00 PST on September 25, 1996. As discussed above, it is likely that these biases result from the use of approximate nitrate boundary conditions and from missing sources of organic carbon in model emissions inventories.

Model input parameter values used to produce the results shown in Figures 2−4 were set at their base case values and were not tuned (within uncertainty ranges) to optimize model performance. The effects of input parameter uncertainty on model predictions are discussed in Section 5.2. Overall the results shown in Figures 2−4 demonstrate excellent agreement between model predictions and measured concentrations of O3/PM1.8 composition and good agreement (to within ± one impactor bin) with respect to the size distribution of particulate matter components.

5.2. Model Uncertainty Analysis. Uncertainty in modeling studies can arise in a number of different areas including model input data (emissions, meteorology, etc) and model formulation (reaction rates, parameterization of processes, etc). A formal uncertainty analysis involves the systematic evaluation of hundreds of different data elements and their impact on the accuracy of model predictions. This process is computationally expensive for complex models involving detailed aerosol operators, and so simplified test cases are often considered instead of full-scale model perturbations. As discussed previously, the Lagrangian form of the CIT air quality model includes a description of all the atmospheric processes contained in the Eulerian model with the exception of vertical advection, vertical wind shear, and horizontal turbulent diffusion. The aerosol predictions shown in Figures 3 and 4 of the current paper are similar to the results produced using the Lagrangian form of the model (*8*). Therefore, vertical advection, vertical wind shear, and horizontal turbulent diffusion are not dominant processes during the episode under consideration, and the results of sensitivity tests performed using the Lagrangian form of the CIT air quality model provide a computationally efficient method for evaluation of the new 3D Eulerian source-oriented external mixture model. The Lagrangian form of the CIT modeling system also has recently undergone several comprehensive uncertainty evaluations (*56*, *57*) that will help to identify key parameters for study in the present analysis. The effect that model formulation and critical input data have on aerosol predictions is analyzed in the sections below.

Input Data − Emissions and Wind Fields. Sensitivity studies carried out using the CIT air quality modeling system applied to the South Coast Air Basin have identified uncertainty associated with input data describing emissions strength and wind strength/direction as the largest contributors to overall uncertainty in model predictions for the concentration of secondary photochemical species such as ozone (*56*). A previous study of these same input parameters determined an uncertainty level of 6% for primary PM2.5 concentrations predicted by the Lagrangian form of the source oriented external mixture air quality model for

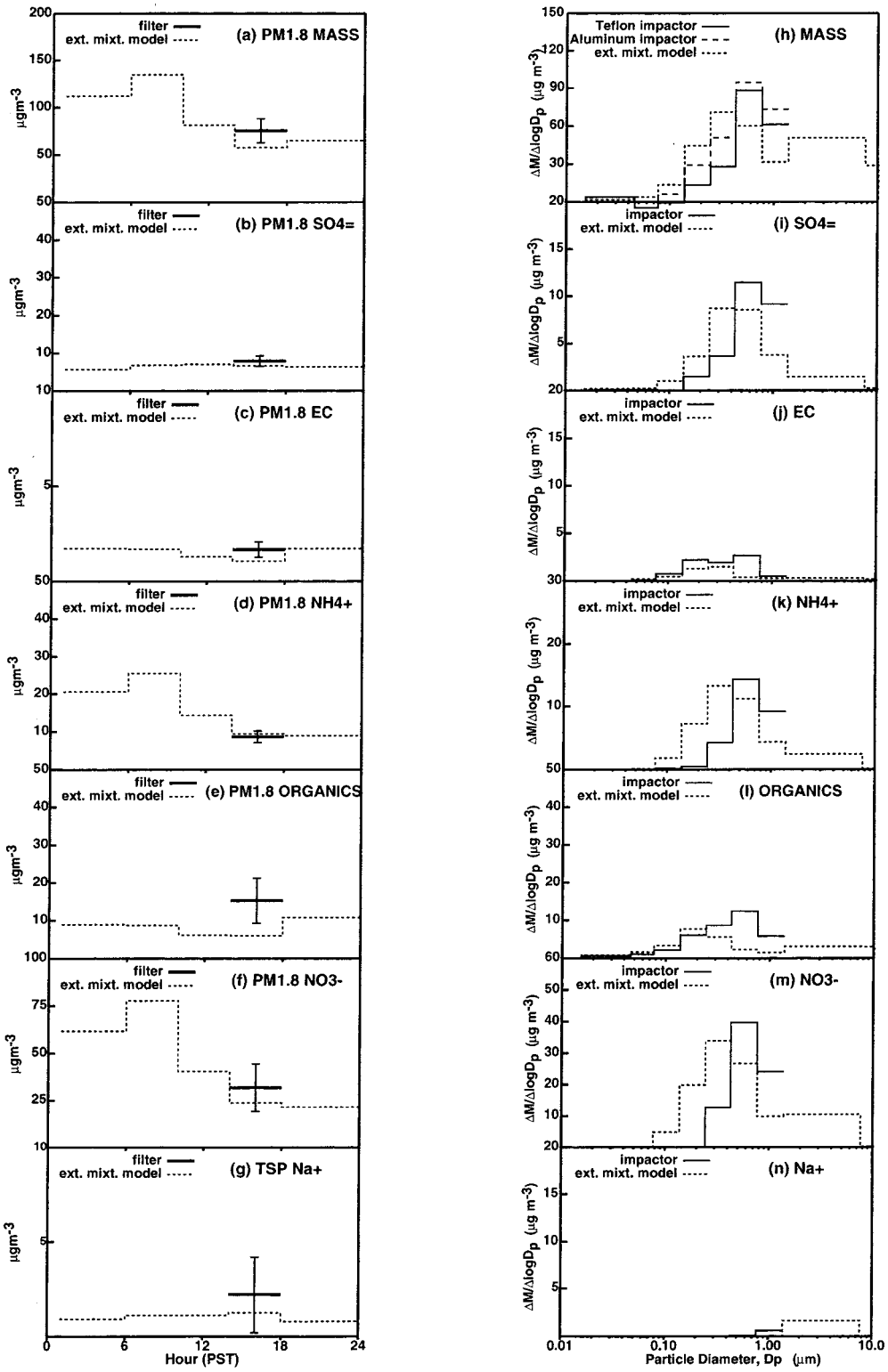

FIGURE 4. Predicted and observed components of airborne particles at Riverside, CA, on September 25, 1996. Panels a−g illustrate the diurnal profile of particle-phase species average concentrations while panels h−n illustrate the size distribution of particle-phase species averaged between 14:00−18:00 h PST. Uncertainty estimates for measured PM1.8 concentrations reflect the difference between collocated filter-based measurements and summed impactor measurements of particle-phase concentrations.

Claremont, CA, on August 28, 1987 (*58*). During that study, 30 alternative air parcel trajectories terminating at the Claremont site at 12:00 PST were integrated backward through wind fields that were perturbed by adding a stochastic uncertainty component to wind vectors. The emissions strength for each source also was treated as a randomly distributed variable with a mean value equal to the nominal inventory value and an uncertainty of ± 30% (minimum value of zero).

In the current study, the perturbation analysis described above is repeated for the air parcel trajectory that arrives at Riverside at 12:00 PST on September 25, 1996. Figure 1b shows 30 alternative trajectory paths arriving at the receptor site that are produced by the methods described above. The

Lagrangian form of the source-oriented external mixture air quality model was used to predict airborne particle concentrations at the receptor site while considering sources along each of these trajectory paths and the effects of uncertainty in source emissions strength. This perturbation study represents the limiting extreme scenario for the modeled episode because alternative air parcel trajectories experience very different emissions conditions as they pass by major combustion point sources that are located in the vicinity of Long Beach. The results of the perturbation analysis indicate that total predicted PM2.5 concentrations at Riverside on September 25, 1996 had an uncertainty of 27%, while primary PM2.5 concentrations had an uncertainty of 19%. This level of uncertainty is considered acceptable considering the extreme nature of the test case.

Model Treatment of Aerosols − Airborne Particle Representation. The current model application represents airborne particulate matter using a discrete particle distribution. Approximately 150 representative particles with known chemical composition and size are tracked through the atmosphere in each grid cell as they evolve through physical and chemical transformations. Appropriate numbers of identical copies of each particle are used to simulate the full airborne particle complex. The accuracy of the discrete particle representation can be evaluated by increasing the number of representative particles to improve the resolution of model calculations. Previous tests (*9*) performed using the Lagrangian form of the source-oriented external mixture air quality model have demonstrated that model results produced using 150 computational particles are virtually identical to those produced using approximately 7000 computational particles. Thus, the discrete particle representation of the airborne particle complex in the current study is accurate.

Model Treatment of Aerosols − Internal vs External Mixture Representations. The internal mixture approximation applied to air quality models results in the blending of particles emitted with different chemical compositions into a single atmospheric particle size distribution. A previous study carried out using a Lagrangian air quality model showed that the internal mixture representation of the atmospheric aerosol could have a large effect on the predicted distribution of chemical components between the gas and particle phases under certain test conditions but that internal mixture predictions for Claremont on August 28, 1987 were essentially identical to external mixture predictions for the same episode (*6*). The 3D Eulerian air quality model described in the current study was executed using both a source-oriented external mixture representation in which the chemically different particles from different sources are tracked separately in the atmosphere and using an internally mixed representation for airborne particles so that the effect of the internal mixture approximation could be directly evaluated. A comparison between internally and externally mixed aerosol results indicates that in this particular application the internal mixture approximation does not have significant adverse effects on the overall predicted composition or size distribution of particulate matter components. Of course only the externally mixed representation of the aerosol is able to track the separate contributions from the different major primary particle sources in a way that is most useful for quick assessment of the effect of emissions controls.

Model Treatment of Aerosols − Coagulation. The time scales for changes to the airborne particle mass distribution through coagulation processing are considerably larger than the corresponding time scales for modification of the airborne particle mass distribution by condensation/evaporation (*6*, *11*). As a result, aerosol coagulation has not been implemented in the 3D model application demonstrated in the current study. To verify that coagulation operators do not significantly affect the predicted size distribution of airborne particulate matter, the Lagrangian form of the source-oriented external mixture air quality model (*6*−*9*) was exercised with an operator that predicted coagulation events between discrete airborne particles based on the Fuch's form of the coagulation coefficient (*59*). When two particle populations experienced coagulation events in the test calculation, the number and mass concentration of the smaller particles was reduced, and the mass concentration of the larger particles was increased. This methodology recognizes that most coagulation events in the atmosphere take place between very small particles (that have a large Brownian velocity) and very large particles (that provide a large target for collision events). The radii of the new combined particles was calculated after the concentration of any particle population decreased by more than 10% or at the end of the 10 min operator splitting step employed in the model calculation. Note that this methodology will provide a direct evaluation of the effect of coagulation on the predicted size and composition distribution of airborne particulate matter, but it will not follow source contributions to airborne particles that have experienced coagulation events.

Aerosol coagulation test calculations were performed for Riverside between the hours of 14:00−18:00 PST on September 25, 1996 using the Lagrangian form of the source-oriented external mixture air quality model. Riverside is a receptor site at the Eastern edge of the air basin where the total time for coagulation events to operate on the aerosol size distribution is approximately 2−3 days during the current study period. Test results indicate that when coagulation processes are included in model calculations, the predicted airborne particle PM10 mass concentration increases from 114 to 115 μg m^{-3}, the mass concentration of accumulation mode aerosols (diameter between 0.1 − 1.0 μm) is unchanged at 58.1 μg m^{-3}, and the mass concentration of ultrafine aerosols (diameter less than 0.1 μm) is reduced from 2 to 1 μg m^{-3}. The net result of coagulation processing is to move a very small amount (approximately 1 μg m^{-3}) of ultrafine particulate matter (diameter less than 0.1 μm) to the coarse particle size range (diameter greater than 1.0 μm), with no significant impact on accumulation mode particles. Thus, the assumption that aerosol coagulation can be neglected when calculating airborne particle mass distributions during the current study seems well justified.

Model Treatment of Aerosols − Nucleation. Nucleation occurs when a condensable gas-phase species is present at concentrations significantly above the saturation concentration, and there is insufficient aerosol surface area for condensation to occur. The aerosol science community generally accepts the concept that nucleation events in urban areas such as Los Angeles usually do not take place because there is a large amount of airborne particulate matter available for condensation processes to occur (*11*). Nucleation in urban areas may occur in rare circumstances such as heavy pollution following a rain event, but those conditions were not encountered in the present study. Thus, the assumption that aerosol nucleation can be neglected when calculating airborne particle mass distributions during the current study seems well justified.

5.3. Regional Contributions to PM2.5 Mass. Figure 5 shows the predicted distribution of PM2.5 mass concentrations in the ground level cell of the modeling domain averaged over each hour of the day on September 25, 1996. Predicted PM2.5 mass concentrations generally increase toward the eastern end of the air basin since it is downwind of the major emissions sources in the Los Angeles area during the current study period. Major sources of ammonia emissions exist in the Chino dairy area located halfway between Fullerton and Rubidoux leading to the formation of large amounts of

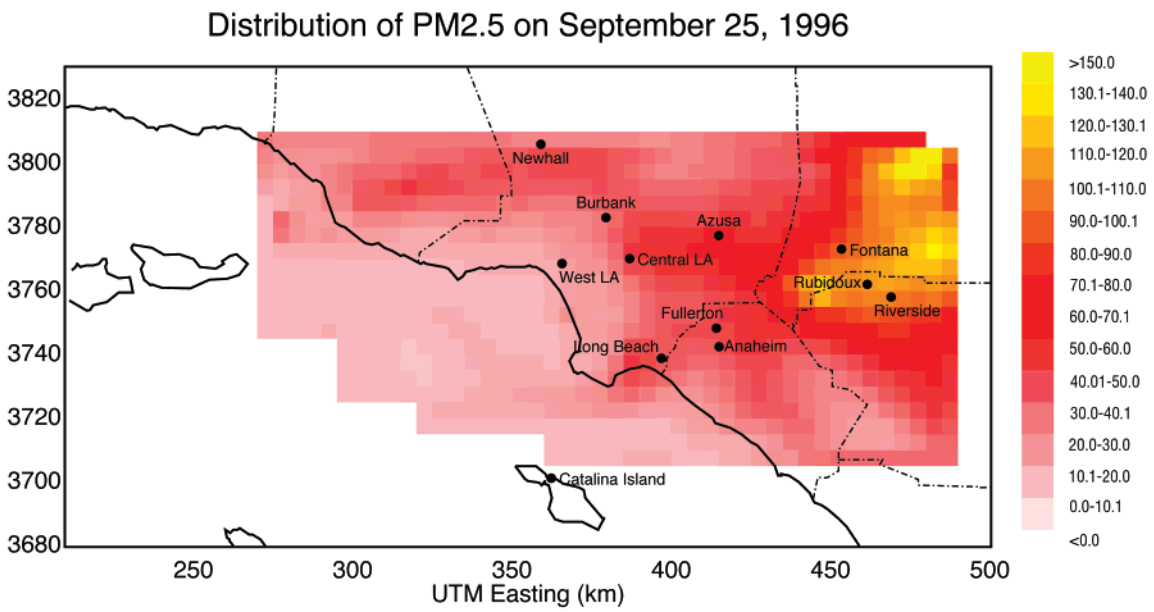

FIGURE 5. Predicted mass concentration of airborne particles with diameter less than 2.5 μm diameter (PM2.5) averaged over each hour of the day on September 25, 1996. Units are μg m^{-3}.

particulate ammonium nitrate in the area east of Chino (*8*). The Long Beach sampling site is located near the upwind edge of the South Coast Air Basin during the episode studied here and thus exhibits relatively low pollutant concentrations, while the Riverside sampling site is located in a relatively polluted downwind area. The predicted maximum 24-h average PM2.5 concentration on September 25, 1996 is 166 μg m^{-3} near the northeast corner of the South Coast Air Basin at 475 Easting 3800 Northing.

Figure 6 separately plots the size and composition distribution of the particles originally released from the 10 externally mixed source categories on September 25, 1996, as they exist in the atmosphere at the Rubidoux air monitoring site shown in Figure 5. The results shown in Figure 6 illustrate that the majority of the PM2.5 mass at this location is associated with secondary ammonium nitrate that has accumulated onto combustion particles and onto hygroscopic background marine particles. These results agree with a previous analysis for Riverside on September 25, 1996 (*8*) and for Claremont on August 28, 1987 (*7*).

The great power of the 3D Eulerian version of the source-oriented external mixture model developed in the current study lies in its ability to expand the analysis shown in Figure 6 to determine the spatial distribution of particle source contributions at a regional scale. Figure 7 shows the predicted distribution of PM2.5 concentrations in the ground level cell of the modeling domain averaged over each hour of the day on September 25, 1996 separated according to the original source of the primary core of each particle. Figure 7a shows that the predicted concentration of airborne crustal particles is highest in the eastern end of the airshed where the majority of the unpaved road travel occurs. Concentrations of PM2.5 crustal particles in the eastern portion of the study domain are typically between 10 and 15 μg m^{-3}, with the grid cell at 475 Easting 3800 Northing registering concentrations of 26 μg m^{-3}.

Figure 7b shows that paved road dust particles are lower in concentration but more broadly distributed than other crustal particles in the South Coast Air Basin. This trend reflects the wide distribution of freeways, surface streets, and the general pattern of urban sprawl in the Los Angeles area. The concentration of PM2.5 paved road dust particles peaks in three general areas: downtown Los Angeles (12 μg m^{-3}), Orange County (13 μg m^{-3}), and east of Fontana (14 μg m^{-3}).

Figure 7c illustrates the regional distribution of airborne particles originally released from diesel engines in the Los Angeles area. The maximum PM2.5 diesel engine particle concentrations are observed off the coast of California in the northwest corner of the study domain and at the Long Beach Harbor. These diesel engine emissions are associated with shipping and other offshore activities and have a peak ambient PM2.5 mass concentration of approximately 16 μg m^{-3}. A peak in the ambient PM2.5 increment having diesel exhaust as the primary particle core also is observed in the northeast corner of the South Coast Air Basin as diesel engine exhaust particles become coated with ammonium nitrate. The fairly high concentration of marine diesel engine particles compared to particles released from on-road heavy-duty diesel engines reflects the relatively concentrated location of the marine emissions as well as the incorporation of cleaner diesel engine technology into the on-road vehicle fleet.

Figures 7d shows that the airborne PM2.5 particles derived from food cooking have a spatial distribution similar to paved road dust particles but at a lower concentration. Three distinct peaks are observed at Los Angeles (4 μg m^{-3}), east of Anaheim (3 μg m^{-3}), and east of Fontana (5 μg m^{-3}). The first two peaks are likely associated with primary emissions, while the last peak is associated with the accumulation of secondary particulate nitrate onto food cooking particles.

Figures 7e,f show that the concentrations of airborne particles released from noncatalyst-equipped gasoline engines and catalyst-equipped gasoline engines have similar patterns reflecting the similar distribution of the underlying emissions within the study domain. The concentration of particles originally released by both types of gasoline engines reaches a maximum value east of Fontana as they become coated with ammonium nitrate. The maximum concentration of particles having a primary particle core emitted from noncatalyst equipped gasoline engines is 13 μg m^{-3}, while the maximum concentration of particles having a primary particle core contributed by catalyst-equipped gasoline engines is only 2.4 μg m^{-3}. This condition results from improvements in emissions control technology used by new

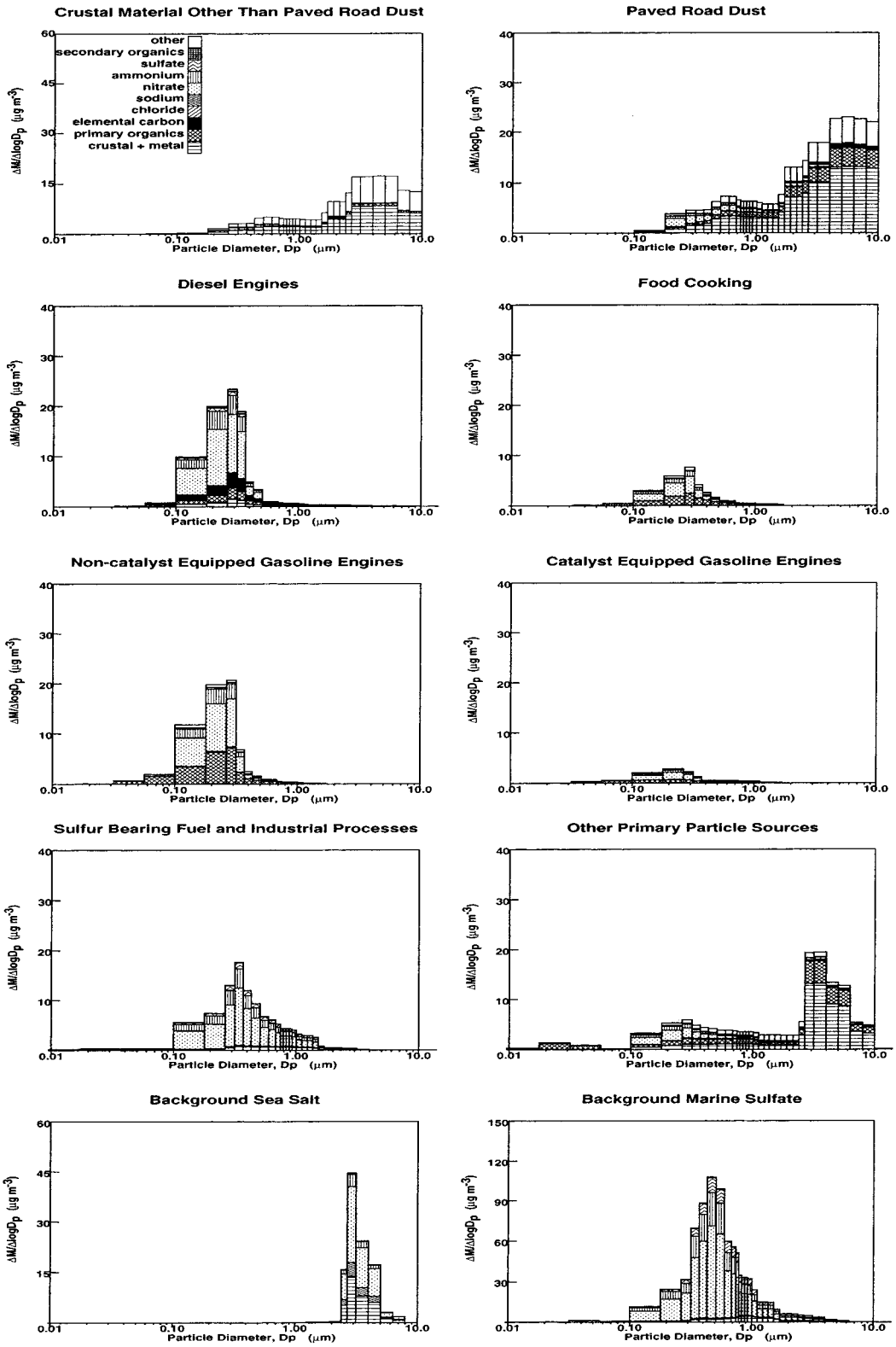

FIGURE 6. Individual source contributions to the airborne particle size and chemical composition distribution at Rubidoux, CA, averaged over each hour of the day on September 25, 1996. Each subplot shows the primary seed particles originally released to the atmosphere along with the gas-to-particle conversion products that have accumulated on those seed particles between their time of release to the atmosphere and their arrival at the receptor site.

catalyst-equipped automobiles and the continued degradation of older noncatalyst-equipped vehicles still being driven in the Los Angeles area.

Figure 7g shows the regional distribution of airborne particles that originate from the combustion of sulfur-bearing fuel and other sulfur oxides sources in the South Coast Air Basin surrounding Los Angeles. Increased concentrations of these particles are apparent in the shipping lanes off the California coast and downwind of refineries located near Hawthorne and Long Beach. A peak concentration of 14 μg

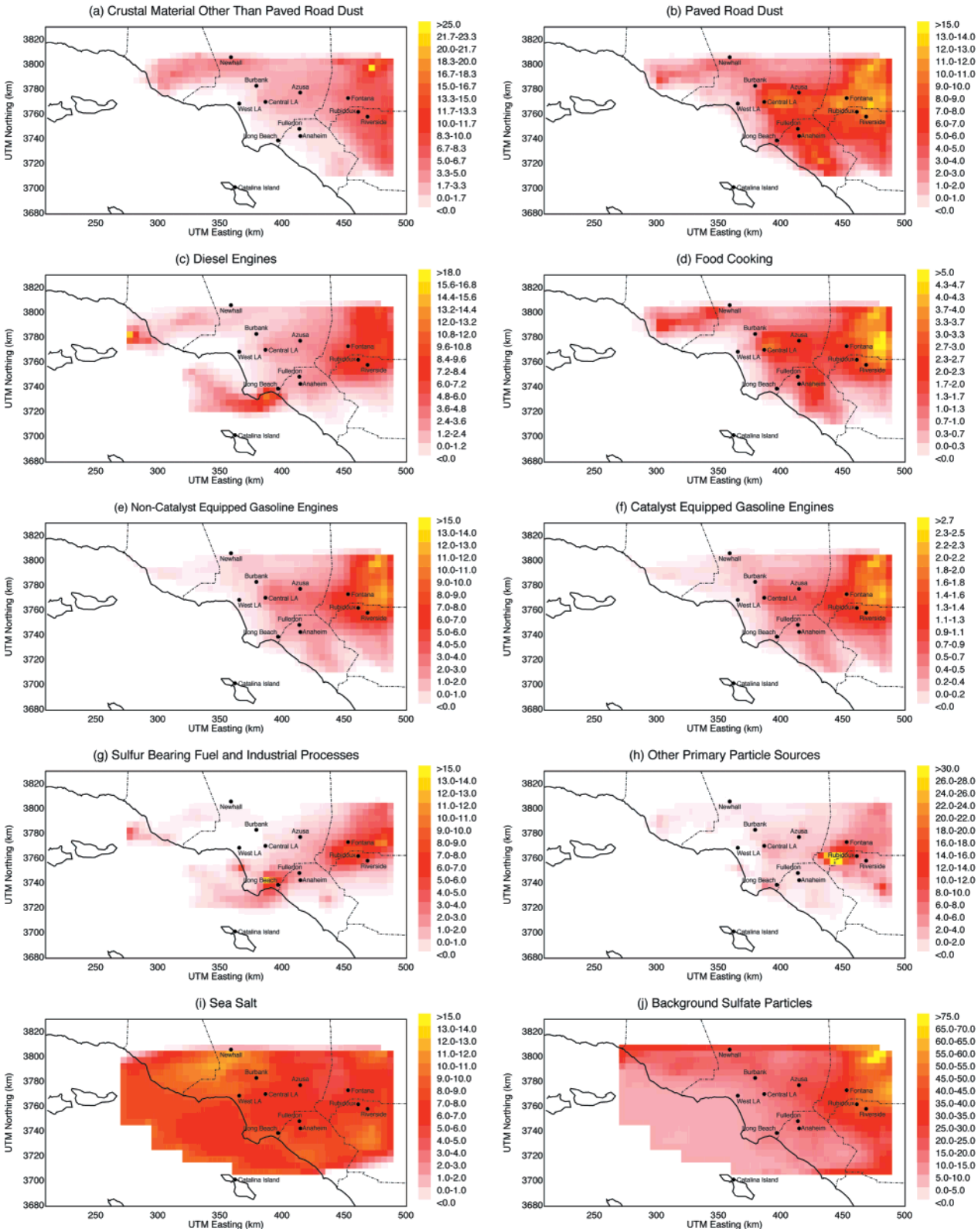

FIGURE 7. Regional concentration of airborne PM2.5 associated with particles having their primary core from crustal material other than paved road dust, paved road dust, diesel engines, food cooking, noncatalyst equipped gasoline engines, catalyst-equipped gasoline engines, combustion of sulfur-containing fuel and industrial processes, other primary particle sources, sea salt, and marine background sulfate particles averaged over each hour of the day on September 25, 1996. PM2.5 contributions include the primary particle core plus all secondary particulate matter that has accumulated on that core since release to the atmosphere. Units are μg m^{-3}.

m^{-3} is predicted near the Long Beach refineries, with a clear plume of high sulfate-content particles predicted downwind from this source area. These particles are hygroscopic and act as a site for the formation of particulate ammonium nitrate by the time that they reach the eastern end of the airshed.

Figure 7h shows the regional distribution of particles released from primary sources other than those described in

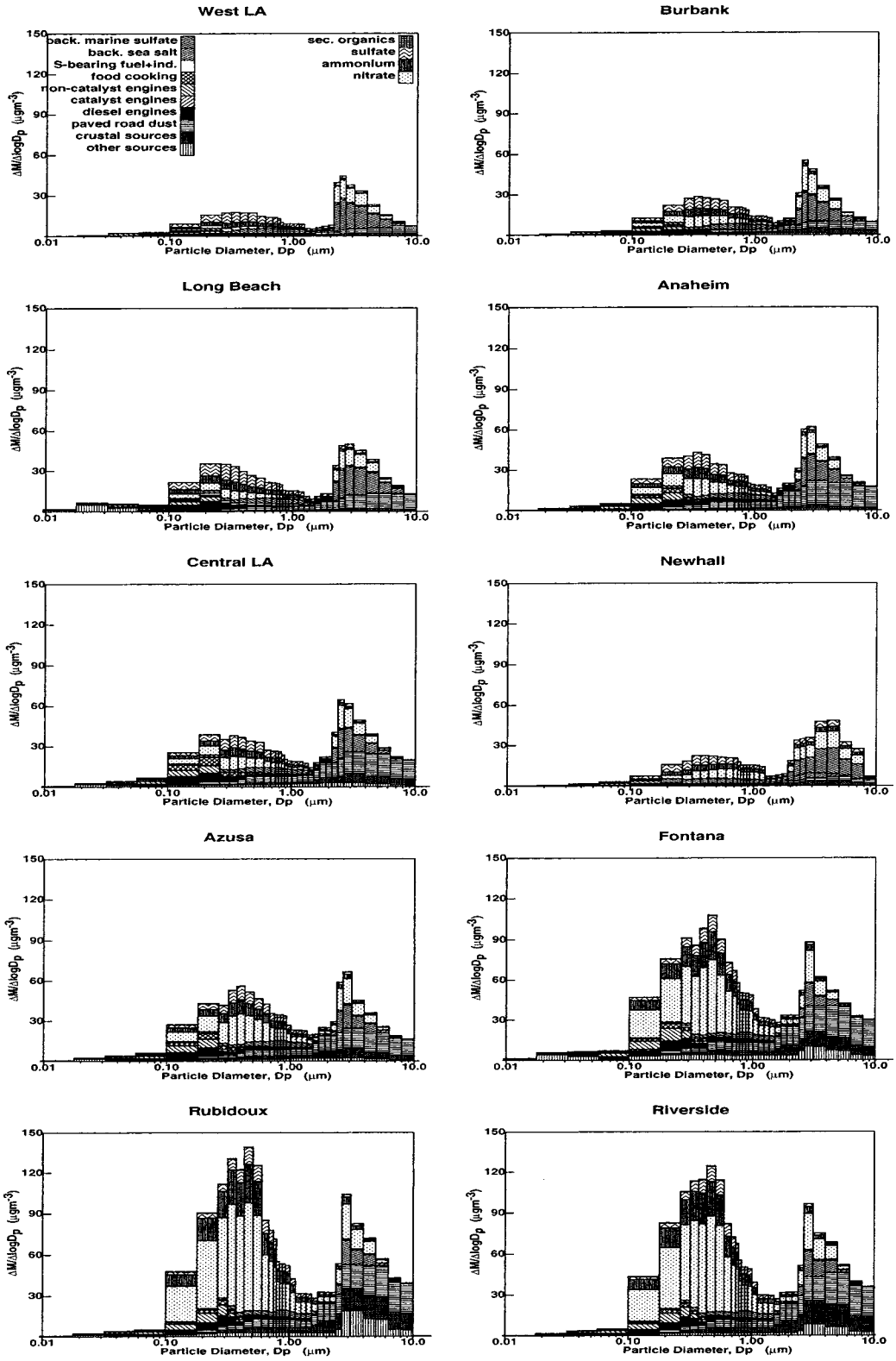

FIGURE 8. Source contributions to the aggregate particle distribution averaged over each hour of the day on September 25, 1996. Each panel shows the primary seed particle concentrations graphed separately from all sulfates, nitrates, ammonium ion, and secondary organic aerosol.

Figures 6a−g. The peak concentration of these particles is 37 μg m^{-3} located west of Rubidoux in an area dominated by agricultural activities.

Figure 7i shows that predicted sea salt particle concentrations are relatively uniform throughout the South Coast Air Basin with concentrations reaching up to 12 μg m^{-3}. Sodium chloride particles originating from the ocean are thermodynamically favored to form sodium nitrate particles in the polluted Los Angeles atmosphere without the involvement for ammonia. As a result, a large concentration spike caused by the formation of additional particulate nitrate on these particles is not observed downwind of the large ammonia emissions sources East of Rubidoux.

Figure 7j shows the predicted concentration of marine background sulfate particles in the study domain after they have accumulated secondary reaction products in the Los Angles atmosphere. As noted previously (*8*) background sulfate particles advected into the Los Angeles area from over the ocean upwind have a size distribution that peaks below 1 μm particle diameter, and so they do not have a large settling velocity. These background sulfate particles are extremely hygroscopic and so they act as a preferential site for the accumulation of secondary ammonium nitrate. The PM2.5 mass concentration of these particles is less than 15 μg m^{-3} on the western edge of the airshed, but through the accumulation of particulate nitrate these particles reach a peak PM2.5 mass concentration of 79 μg m^{-3} in the northeastern portion of the South Coast Air Basin.

Figure 8 shows the airborne particle size distribution at each of the monitoring sites shown in Figure 5 broken down according to source type. Primary particulate matter (released directly from a source in the particle phase) is graphed separately from all particle-phase sulfates, nitrates, ammonium ion, and secondary organic aerosol. Model predictions show the buildup of significant amounts of ammonium nitrate aerosol in the eastern portion of the air basin primarily in the size range below 1 μm particle diameter. These results emphasize that the majority of the elevated PM2.5 concentration in the eastern half of the South Coast Air Basin (shown in Figures 5 and 7) is associated with secondary particulate matter, not primary particle emissions.

6. Discussion

Predicted and measured peak 1-h average ozone concentrations during the September 1996 period studied here were generally less than 100 ppb, which is considerably lower than historically observed values in the Los Angeles area in September. In contrast, the predicted regional PM2.5 mass concentration in the South Coast Air Basin more than doubled the current standard of 65 μg m^{-3}. This trend illustrates the changing nature of air quality problems in Los Angeles, and it suggests that future control strategies designed to improve air quality in Los Angeles must include an emphasis on fine particle control.

The greatest contribution to regional PM2.5 mass concentrations in the South Coast Air Basin surrounding Los Angeles on September 25, 1996 is associated with the accumulation of secondary ammonium nitrate on marine background marine sulfate particles (see Figure 6 in current paper and Figures 5 and 6 in ref *8*). This pattern indicates that control of regional PM2.5 concentrations in Los Angeles must be accomplished through a program that includes reductions in the emissions of gaseous precursors to secondary PM2.5 in addition to the more obvious primary fine particle controls (*9*).

The exact source of the background marine sulfate particles observed at San Nicolas Island during 1987 (*6*, *7*) and at Santa Catalina Island in 1996 (*8*) is not known. The size distribution of these particles has a maximum below 1 μm particle diameter, suggesting that a chemical or biological source produced these particles rather than a mechanical source such as breaking waves. One possible source of the background marine sulfate particles is combustion of high sulfur content fuel from off-shore shipping or from industrial processes outside California (the sulfur content of fuel used in California is strictly regulated). Another possible source of background marine sulfate particles is the oxidation of DMS is ocean surface waters. Future studies will try to identify the source origin of these particles.

Acknowledgments

This research was supported by the United States Environmental Protection Agency under contract # R826371-01-0.

Literature Cited

(1) Schwartz, J.; Dockery, D. W.; Neas, L. M. *J. Air Waste Management Assoc.* **1996**, *46*, 927−939.
(2) Klemm, R. J.; Mason, R. M.; Heilig, C. M.; Neas, L. M.; Dockery, D. W. *J. Air Waste Management Assoc.*. **2000**, *50*, 1215−1222.
(3) Richards, L. W.; Alcorn, S. H.; McDade, C.; Couture, T.; Lowenthal, D.; Chow, J. C.; Watson, J. G. *Atmos. Environ.* **1999**, *33*, 4787−4795.
(4) Kleeman, M. J.; Eldering, A.; Cass, G. R. *Environ. Sci. Technol.* **2001**, In press.
(5) *Climate change 1995. The science of climate change*; Houghton, J. T., Meira Filho, L. G., Callandar, B. A., Harris, N., Lattenberg, A., Maskell, K., Eds.; Cambridge University Press: Cambridge, U.K., 1996.
(6) Kleeman, M. J.; Cass, G. R.; Eldering, A. *J. Geophys. Res.* **1997**, *102*, 21355−21372.
(7) Kleeman, M. J.; Cass, G. R. *Atmos. Environ.* **1998**, *33*, 177−189.
(8) Kleeman, M. J.; Hughes, L. S.; Allen, J. O.; Cass, G. R. *Environ. Sci. Technol.* **1999**, *33*, 4331−4341.
(9) Kleeman, M. J.; Cass, G. R. *Environ. Sci. Technol.* **1999**, *33*, 177−189.
(10) Goodin, W. R.; McRae, G. J.; Seinfeld, J. H. *Bull. Am. Meteorological Soc.* **1976**, *57*, 646−647.
(11) Wexler, A. S.; Lurmann, W. L.; Seinfeld, J. H. *Atmos. Environ.* **1994**, *28*, 531−546.
(12) Meng, Z. Y.; Dabdub, D.; Seinfeld, J. H. *J. Geophys. Res.* **1998**, *103*, 3419−3435.
(13) Lurmann, F. W.; Wexler, A. S.; Pandis, S. N.; Musarra, S.; Kumar, N.; Seinfeld, J. H. *Atmos. Environ.* **1997**, *31*, 2695−2715.
(14) Potukuchi, S.; Wexler, A. S. *Atmos. Environ.* **1997**, *31*, 741−753.
(15) Sun, Q.; Wexler, A. S. *Atmos. Environ.* **1998**, *32*, 3533−3545.
(16) Middleton, P. *J. Air Waste Management Assoc.* **1997**, *47*, 302−316.
(17) Jacobson, M. Z. *Atmos. Environ.* **1997**, *31*, 131−144.
(18) Pai, P.; Vijayaraghavan, V.; Seigneur, C. *J. Air Waste Management Assoc.* **2000**, *50*, 32−42.
(19) Binkowski, F. S.; Shankar, U. *J. Geophys. Res.* **1995**, *100*, 26191−26209.
(20) Ackerman, I. J.; Hass, H.; Memmesheimer, M.; Ebel, A.; Binkowski, F. S.; Shankar, U. *Atmos. Environ.* **1998**, *32*, 2981−2999.
(21) Jacobson, M. Z. *Nature* **2001**, *409*, 695−697.
(22) Reynolds, S. D.; Roth, P. M.; Seinfeld, J. H. *Atmos. Environ.* **1973**, *7*, 1033−1061.
(23) Reynolds, S. D.; Liu, M.; Hecht, T. A.; Roth, P. M.; Seinfeld, J. H. *Atmos. Environ.* **1974**, *8*, 563−596.
(24) Roth, P. M.; Roberts, P. J.; Liu, M.; Reynolds, S. D.; Seinfeld, J. H. *Atmos. Environ.* **1974**, *8*, 97−130.
(25) Reynolds, S. D.; Seinfeld, J. H. *Environ. Sci. Technol.* **1975**, *9*, 433−447.
(26) McRae, G. J.; Seinfeld, J. H. *Atmos. Environ.* **1983**, *17*, 501−522.
(27) McRae, G. J.; Goodin, W. R.; Seinfeld, J. H. *Atmos. Environ.* **1982**, *16*, 679−696.
(28) Falls, A. H.; Seinfeld, J. H. *Environ. Sci. Technol.* **1978**, *12*, 1398−1406.
(29) Falls, A. H.; McRae, G. J.; Seinfeld, J. H. *Intl. J. Chem. Kinetics XI* **1979**, 1137−1162.
(30) Goodin, W. R.; McRae, G. J.; Seinfeld, J. H. *J. Appl. Meteorol.* **1979**, *18*, 761−771.
(31) Goodin, W. R.; McRae, G. J.; Seinfeld, J. H. *J. Appl. Meteorol.* **1980**, *19*, 98−108.
(32) Russell, A. G.; McCue, K. F.; Cass, G. R. *Environ. Sci. Technol.* **1988**, *22*, 263−270.
(33) Russell, A. G.; McCue, K. F.; Cass, G. R. *Environ. Sci. Technol.* **1988**, *22*, 1336−1347.
(34) Milford, J. B.; Russell, A. G.; McRae, G. J. *Environ. Sci. Technol* **1989**, *23*, 1290−1301.
(35) Russell, A. G.; St. Pierre, D.; Milford, J. B. *Science* **1990**, *247*, 201−205.
(36) McNair, L. A.; Russell, A. G.; Odman, M. T. *J. Air Waste Management Assoc.* **1992**, *42*, 174−178.
(37) Russell, A. G.; Winner, D. A.; Harley, R. A.; McCue, K. F.; Cass, G. R. *Environ. Sci. Technol.* **1993**, *27*, 2772−2782.
(38) Harley, R. A.; Russell, A. G.; Cass, G. R. *Environ. Sci. Technol.* **1993**, *27*, 1638−1649.
(39) Harley, R. A.; Russell, A. G.; McRae, G. J.; Cass, G. R., Seinfeld, J. H. *Environ. Sci. Technol.* **1993**, *27*, 378−388.
(40) Wexler, A. S.; Seinfeld, J. H. *Atmos. Environ.* **1991**, *25A*, 2731−2748.
(41) Pandis, S. N.; Harley, R. A.; Cass, G. R.; Seinfeld, J. H. *Atmos. Environ.* **1992**, *26A*, 2269−2282.
(42) Gasdag, J. *J. Computational Phys.* **1973**, *12*, 100−113.

(43) Chock, D. *Atmos. Environ*. 1991, *25*, 853−871.
(44) Odum, J. R.; Hoffmann, T.; Bowman, R.; Collins, E.; Flagan, R. C.; Seinfeld, J. H. *Environ. Sci. Technol.* **1996**, *30*, 2580−2585.
(45) Holtzworth, G. C. *J. Appl. Meteorol.* **1967**, *6*, 1029−1044.
(46) Hughes, L. S.; Allen, J. O.; Kleeman, M. J.; Johnson, R. J.; Cass, G. R.; Gross, D. S.; Gard, E. E.; Galli, M. E.; Morrical, B. D.; Fergensen, D. P.; Dienes, T.; Noble, C. A.; Liu, D.; Silva, P. J.; Prather, K. A. *Environ. Sci. Technol*. **1999**, *33*, 3506−3515.
(47) Fraser, M. P.; Grosjean, D.; Grosjean, E.; Rasmussen, R. A.; Cass, G. R. *Environ. Sci. Technol.* **1996**, *30*, 1731−1743.
(48) de Leeuw, G.; Neele, F. P.; Hill, M.; Smith, M. H.; Vignati, E. *J. Geophys. Res.* **2000**, *105*, 29397−29409.
(49) Grosjean E.; Grosjean, D.; Fraser, M. P.; Cass, G. R. *Environ. Sci. Technol*. **1996**, *30*, 2687−2703.
(50) Eldering, A.; Cass, G. R. *J. Geophys. Res.* **1996**, *101*, 19343−19369.
(51) Hildemann, L. M.; Markowski, G. R.; Cass, G. R. *Environ. Sci. Technol.* **1991**, *25*, 744−759.
(52) Schauer, J. J.; Kleeman, M. J.; Cass, G. R. *Environ. Sci. Technol*. **1999**, *33*, 1578−1587.
(53) Schauer, J. J.; Kleeman, M. J.; Cass, G. R.; Simoneit, B. R. T. *Environ. Sci. Technol.* **2001**, submitted for publication.
(54) Harley, R. A.; Hannigan, M. P.; Cass, G. R. *Environ. Sci. Technol.* **1992**, *26*, 2395−2408.
(55) Gharib, S.; Cass, G. R. *Ammonia emissions in the South Coast Air Basin;* open file report 84-2; Environmental Quality Laboratory, California Institute of Technology: Pasadena, CA, 1984.
(56) Bergin, M. S.; Noblet, G. S.; Petrini, K., Dhieux, J. R., Milford, J. B., Harley, R. A. *Environ. Sci. Technol.* **1999**, *33*, 1116−1126.
(57) Bergin, M. S.; Milford, J. B. *Atmos. Environ*. **2000**, *34*, 781−792.
(58) Kleeman, M. J.; Cass, G. R. *Atmos. Environ*. **1999**, *33*, 4597−4613.
(59) Fuchs, N. A. *Mechanics of Aerosols;* Pergamon: New York, 1964.

Received for review April 23, 2001. Revised manuscript received September 4, 2001. Accepted September 6, 2001.

ES010886M